Heliyon 10 (2024) e40625

Contents lists available at ScienceDirect

Heliyon

journal homepage: www.cell.com/heliyon

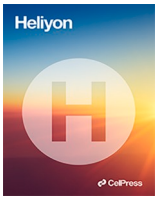

Research article

Simultaneous nitric oxide and toluene reduction over Pt-based catalyst

Cheonwoo Jeong [a,*], Dongcheol Lee [a], Sungjoong Kim [b], Joon Hyun Baik [c], Joonwoo Kim [a]

[a] *Industrial Gas Research Cell, Research Institute of Industrial Science & Technology (RIST), 187-12, Geumho-ro, Gwangyang-si, Jeollanam-do, 57801, Republic of Korea*

[b] *Environment Infra Section, Research Institute of Industrial Science & Technology (RIST), 187-12, Geumho-ro, Gwangyang-si, Jeollanam-do, 57801, Republic of Korea*

[c] *Department of Chemical and Biological Engineering, Sookmyung Women's University, 100 Cheongpa-ro 47-gil, Yongsan-gu, Seoul, 04310, Republic of Korea*

A B S T R A C T

This research investigates the simultaneous reduction of nitric oxide (NOx) and toluene using Pt-based catalysts, aiming at applications in small-scale industrial environmental processes. Catalysts with varying Pt loadings from 0.01 to 3 % were synthesized through wet impregnation, and their dispersion was assessed across several characterizations, revealing effective Pt dispersion even at loadings above 1 %. Under conditions of high toluene feed, the 3 % Pt-loaded catalyst emerged as the most efficient, achieving significant NOx and toluene conversion rates. The performance of this catalyst was thoroughly examined under various operational parameters including NO, toluene, O_2 concentrations, gas hourly space velocity (GHSV) and reaction temperature. A short-stress test further underscored its effectiveness, with NOx and toluene conversions reaching 89.7 % and 97.6 %, respectively. Additionally, a preliminary process simulation of the NOx reduction by toluene indicated an energy efficiency improvement of over 8 % compared to conventional RCO and de-NOx processes. The findings suggest the catalyst's potential for NOx reduction in industrial settings, utilizing toluene present in flue gas without the need for additional commercial reducing agents.

1. Introduction

The urgency of addressing emissions of nitrogen oxides and volatile organic compounds (VOCs) has intensified, becoming a focal point in environmental and public health debates, particularly due to the significant contributions from diesel engines and industrial plants [1–9]. NOx, recognized as primary air pollutants, not only exacerbate respiratory diseases but also considerably impact ecosystems, contributing to the development of ground-level ozone and acid rain [9–17]. Concurrently, VOCs emitted during various industrial processes and from certain types of fuel aggravate these issues [18,19]. In the atmosphere, VOCs react with NOx and ozone, leading to the formation of particulate matter, which further deteriorates air quality and poses additional health risks [7,8,16,20–23]. These environmental and health impacts have prompted governments to enforce stricter regulations aimed at controlling these emissions, thereby mitigating the adverse effects of these pollutants and spurring the development of more efficient and cleaner technologies in industrial processes and engine designs [7,24–26]. The implementation of these regulations is a critical step toward reducing the environmental footprint of industrial activities and improving public health outcomes.

Selective Catalytic Reduction (SCR) has become a primary method for NOx removal, offering a significant reduction in these highly reactive gases known for their environmental impact. This technology's effectiveness stems from its significant reduction in NOx

* Corresponding author.
E-mail address: cjeong@rist.re.kr (C. Jeong).

https://doi.org/10.1016/j.heliyon.2024.e40625
Received 3 September 2024; Received in revised form 18 October 2024; Accepted 20 November 2024
Available online 21 November 2024

emissions. However, SCR depends on reductants such as NH_3 or urea, which are necessary because NOx gases cannot be adequately reduced by the flue gas alone [27–29]. Despite ammonia's efficacy as a reductant, its highly toxic nature requires extensive safety measures, including the installation of leakage detection sensors and scrubbers for residual gas removal during emergencies [30]. Consequently, the use of NH_3 incurs significant financial and operational burdens due to the need for ongoing maintenance and monitoring of these safety systems.

Alongside SCR, various methods have been developed for VOCs removal, emitted from different industrial processes and known contributors to air pollution and smog formation. These include thermal oxidation, regenerative thermal oxidation (RTO), and regenerative catalytic oxidation (RCO) [31,32]. A common requirement among these techniques is high temperatures to initiate VOCs oxidation, even during catalytic reactions. The thermal oxidation process, characterized by high operational temperatures, is hindered by low energy efficiency due to the substantial energy demand for maintaining these temperatures. RTO was developed to improve this process's efficiency by concentrating VOCs, enabling combustion at a reduced flow rate [33]. In contrast, RCO operates at lower temperatures compared to RTO, enhancing its overall efficiency. However, the implementation of these technologies entails significant financial costs [34,35]. The installation and maintenance of systems capable of high-temperature operations or those equipped with advanced catalytic materials represent considerable investments. Additionally, the operational costs associated with energy consumption, especially for thermal and regenerative thermal oxidation processes, contribute to the overall expenditure [36]. For many industries, particularly smaller operations, these costs can be prohibitively high, limiting the widespread adoption of these environmentally beneficial technologies.

In industrial environments such as drum manufacturing plants or car painting shops, paint is applied to products and dried using heat from combustion processes, emitting VOCs from the paint and NOx from combustion [32,37–40]. Large-scale facilities can manage these emissions using environmental processes like SCR, RTO, or RCO [41–44]. However, smaller shops often find it financially unfeasible to invest in such equipment, resulting in the uncontrolled release of these pollutants without any capture or reduction measures.

In these applications, using the SCR process with NH_3 is not straightforward. Firstly, these sites are usually close to residential areas rather than industrial zones, making the use of chemicals such as NH_3 undesirable. Even a small release of NH_3 can easily indicate a problem with the process or instruments. Secondly, controlling NH_3 requires additional government licensing, leading to financial burdens such as the operation and maintenance costs of storage and handling equipment for NH_3. Finally, NH_3 can cause significant erosion problems. In natural gas applications, there is notable corrosion in steel piping systems due to NH_3, leading to material degradation and potential failures [45]. For these reasons, using NH_3 in small shop applications is quite challenging.

Therefore, it would be beneficial to use VOCs as a reducing agent to reduce NOx emissions without the need for additional NH_3 injection. In literature, several types of catalyst such as Cu, Pt, Co and Ag based zeolite were reported that it reduces NOx by small size of gas molecule hydrocarbon such as CO, CH_4, C_2H_4 or C_3H_6 [46]. In this report, reaction mechanism of NOx reduction by hydrocarbon is suggested that intermediate species of hydrocarbon can reacted with NOx and converted into N_2 [46]. In mobile applications, several researchers have focused on reducing both VOCs and NOx. For instance, the Peugeot research center reported that hydrocarbons such as decane, ethanol, and ULSD (classical diesel fuel) can be used as reducing agents to decrease NOx. In this study, De-NOx test was conducted over Ag-based catalyst and its performance was 85 % for ethanol, 67 % for decane, and 43 % for ULSD, respectively [47]. Additionally, another research group explored a different approach where NOx was controlled using onboard NH_3 production over a three-way catalyst (TWC) for subsequent storage [48]. However, this concept still requires NH_3 injection at different intervals. Furthermore, several studies have reported that NO and hydrocarbons can be reduced over V-based catalysts with NH_3 as the reducing agent; however, these catalysts cannot decrease NO without NH_3 [49–51].

In this study, we explored a catalyst that simultaneously removes NOx and VOCs without additional NH_3 injection. Although numerous studies have been conducted on this technology, one of the primary limitations is its relatively low de-NOx performance and narrow operational temperature window compared to conventional methods. Over recent decades, various active catalysts such as Ag or Au have been investigated. However, Pt-based catalysts are more practical options for application in smaller sites. We synthesized a Pt-based catalyst supported on La-promoted γ-Al_2O_3 in varying Pt amounts. The prepared catalysts were characterized using various techniques, including Brunauer-Emmett-Teller (BET), X-ray fluorescence (XRF), inductively coupled plasma atomic emission spectroscopy (ICP-AES), powder X-ray diffraction (XRD), and transmission electron microscopy (TEM). Toluene, commonly used as a solvent in commercial processes, was selected as the model compound of VOCs. We investigated the performance of NOx and VOCs removal over the catalyst in a fixed-bed reactor. Additionally, we conducted short stress test with characterizations of used catalyst. Finally, we also made preliminary process model of this simultaneous reduction of NOx and toluene compared to conventional process which is combined with RCO and NH_3 SCR.

2. Experimentals

2.1. Catalyst preparation

The catalysts were synthesized using the wet impregnation method. Initially, Pt precursor solutions were prepared by dissolving H_2PtCl_6 (Sigma-Aldrich) in distilled water to attain concentrations of 0.01 %, 0.05 %, 0.5 %, 1 %, and 3 %. These specific concentrations were based on a reference amount of 10 g of La-stabilized alumina powder, used as the support material. The La-stabilized alumina powder was placed into a flask, followed by the addition of the respective Pt precursor solution. The mixture was then subjected to a 30-min homogenization process to ensure thorough and even distribution of the solution.

Throughout the process, continuous dispersion was maintained with the homogenizer. Tetraethylammonium hydroxide was

incrementally added to the mixture until pH 10 to control particle size [52–57]. This was followed by a 30-min stirring period to stabilize pH. The process was further continued by adding malic acid dropwise until pH 6, which was again followed by an additional 30 min of stirring for pH stabilization.

After achieving the required pH stability, the solution was calcined in a muffle furnace at 400 °C for over 6 h. Then the sample was crushed to yield the final Pt alumina catalyst. The catalysts were labeled as 0.01PtA, 0.05PtA, 0.5PtA, 1PtA, and 3PtA, corresponding to their respective Pt contents.

2.2. Characterization

The crystal structural properties of the synthesized catalysts were analyzed using XRD (Rigaku Dmax-2500V/PC X-Ray diffractometer system, 45 kV and 40 mA, Tokyo, Japan). Diffractograms were recorded over a 2θ range of 10°–80° using Cu Kα radiation as the X-ray source with a wavelength of 1.54 Å.

BET surface area measurements were performed using an ASAP 2010 (Micromeritics, USA). Prior to the measurement, a sample of 0.4 g was pretreated at 200 °C overnight under vacuum conditions.

CO chemisorption experiments were carried out using a Bel Japan Belcat II equipped with a Thermal Conductivity Detector (TCD). A 50 mg sample was placed in the cell and preheated at 450 °C for 20 min, followed by cooling to 50 °C. A loop filled with 10 % CO/He, having a volume of 0.974 cm^3, was used for the measurement. The dosing time was set to 60 s, and the purge time was 15 s. TCD peak signals reached saturation after three injections, and the last three peaks were utilized for calibration of the CO adsorption amount.

To determine the metal content in the catalysts, both XRF and ICP-AES were performed. The XRF analysis was conducted using an ZSX Primus instrument, operated at 60 kV and 150 mA (Rigaku, Japan). For the ICP-AES analysis, samples were measured by SPECTRO ARCOS (AMETEK, Germany).

2.3. Catalytic activity tests

The prepared sample was loaded into a tubular reactor with dimensions of 5 cm in diameter and 60 cm in length. To generate the feed gas, mass flow controllers were utilized to adjust to the desired reaction conditions using high-purity gases. Oxygen (O_2, 99.999 %), carbon dioxide (CO_2, 99.999 %), and nitrogen (N_2, 99.999 %) gases, along with a 5 % NO/N_2 balance mixture, were sourced from Sinil Gas in Gwangju City, South Korea. Toluene (Samchun Chemical Co Ltd, Gangnam-gu, Seoul, South Korea) was introduced into a 250 mL vapor chamber via an HPLC pump and maintained at 40 °C by a heating jacket. Saturated toluene vapor, purged with N_2, was then mixed with the feed gas.

The reactor temperature was regulated by an electric heater, with temperature control managed by a Yokogawa controller. The levels of nitric oxides (NO, N_2O and NO_2) in the effluent were measured using an infrared spectroscopy system, Nicolet 6700 FT-IR spectrometer (Thermo Fisher Scientific, USA), which featured a 2 m gas cell (Thermo Nicolet, USA) equipped with an MCT detector. Additionally, toluene was monitored as total hydrocarbon (THC) using a emission THC analyzer, Polaris FID model (Pollution, Italy), based on a flame ionization detector (FID).

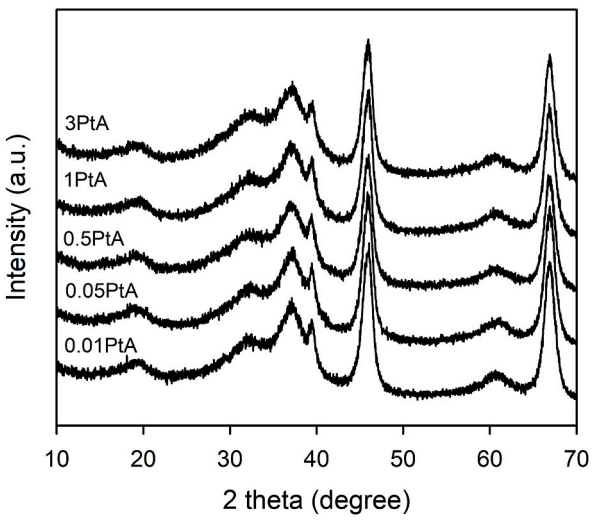

Fig. 1. XRD patterns of prepared catalysts.

3. Results and discussion

3.1. Catalyst characterization

The crystal structural properties of the catalysts were elucidated using powder XRD, as depicted in Fig. 1. The XRD patterns of the catalysts revealed several distinct reflections at characteristic angles: $2\theta = 19.5^\circ$, 31.9°, 37.6°, 39.5°, 45.9°, 60.9°, and 67.0°. These angles correspond to the {111}, {220}, {311}, {222}, {400}, {511} and {440} lattice planes of γ-Al_2O_3, respectively, in alignment with the PDF 10–0425 [58–60]. Interestingly, no reflections directly related to La or Pt were observed in the XRD patterns of any of the catalyst samples. This absence might be attributed to the low concentration of these compounds, falling below the detection limit of the XRD study. This finding is consistent with the literature, which indicates that Pt reflections typically appear only at loadings above 5 % [61]. However, it can be inferred that the particles enriched with La and Pt did not undergo significant aggregation during the catalyst preparation process. This suggests a high likelihood that these compounds were well-dispersed over the catalyst surface.

Table 1 presents the textural properties of the prepared catalysts, as determined by N_2 adsorption-desorption isotherms. The BET surface area of these catalysts remained relatively consistent, with only minor variations observed within the range of 148–151 m^2/g. However, the introduction of Pt onto Al_2O_3 led to noticeable changes in pore characteristics. Specifically, a gradual decrease in pore volume was observed as the Pt loading increased, with values ranging from 0.87 cm^3/g for the catalyst designated as 0.01PtA to 0.71 cm^3/g for the catalyst labeled as 3PtA. This trend aligns with literature findings, which suggest that Pt particles can occupy some of the pores of Al_2O_3, leading to reductions in BET surface area and pore volume [62,63]. This trend was accompanied by a corresponding reduction in pore diameter, which diminished from 20.0 nm in the case of 0.01PtA to 17.7 nm for 3PtA.

To investigate the characteristics of Pt particles, CO chemisorption experiments were conducted, and the results are summarized in Table 2. This technique is widely used to assess the size and dispersion of Pt supported catalyst [64]. The premise of the experiment is based on the understanding that CO adsorbs onto Pt in a 1:1 stoichiometry, and the properties related to Pt are deduced from this fundamental interaction. The data reveals that the amount of CO adsorption increases proportionally with the Pt content, ranging from 0.01 cm^3/g for 0.01PtA to 1.24 cm^3/g for 3PtA, following a trend similar to that reported in the literature [65]. However, the calculation of Pt dispersion takes into account this adsorption amounts relative to the total actual amount of Pt present. Therefore, for the catalyst 0.01PtA, an exceptionally high Pt dispersion of 70.4 % was observed, indicating a more evenly distributed Pt presence. In contrast, as the amount of Pt increases, the dispersion decreases; the catalyst 3PtA displayed a lower dispersion rate of 35.9 %. This trend aligns with the increase in Pt particle size, which is found to grow from 1.6 nm for 0.01PtA to 3.2 nm for 3PtA, as shown in Table 2.

Table 3 presents the elemental analysis results for the prepared catalysts, as determined by XRF and ICP-AES. While XRD analysis did not reveal the presence of Pt species, Pt was found in catalyst by XRF and ICP-AES analysts. For XRF result, the measured Pt loadings closely align with the intended concentrations: 0.02 wt% for 0.01PtA, 0.06 wt% for 0.05PtA, 0.50 wt% for 0.5PtA, 0.95 wt% for 1PtA, and 3.36 wt% for 3PtA. The slightly higher Pt loading observed for the 3PtA sample may be due to measurement variability inherent in the XRF technique. To validate these findings, ICP-AES analysis was performed, yielding results that were consistent with the XRF measurements. These findings suggest that the Pt impregnation onto the Al_2O_3 support was effectively achieved, with minimal loss of the precursor material during the catalyst preparation steps.

Fig. 2 presents TEM images of 0.5PtA, 1PtA, and 3PtA catalysts, alongside the Pt particle size distribution for these samples. For samples with low Pt content (0.01PtA and 0.05PtA), the TEM images shown in Figs. S1a and S1b did not reveal any aggregated particles. However, for samples with higher Pt loading, segregated particles were quantified using the scale bar on the images, and their distribution is depicted in Fig. 2d. With an increase in Pt content within the catalyst, there was a noticeable shift in the particle size distribution towards larger sizes. Specifically, the average particle sizes for the 0.5PtA, 1PtA, and 3PtA catalysts were measured to be 1.3, 1.4, and 2.0 nm, respectively. Additionally, images of different regions of the 1PtA and 3PtA samples, shown in Figs. S1c and S1d, revealed average particle sizes of 1.4 nm and 1.8 nm, respectively. This increase in particle size with higher Pt loading is consistent with the trends observed in the CO chemisorption analysis, as detailed in Table 2.

Table 1
BET surface area, pore volume and pore diameter of catalysts.

Sample	SA_{BET} (m^b/g) [a]	Vp (cm^c/g) [b]	dp (nm) [c]
0.01PtA	149	0.87	20.0
0.05PtA	151	0.85	19.9
0.5PtA	150	0.86	19.8
1PtA	149	0.84	19.6
3PtA	148	0.71	17.7

[a] The BET surface area was calculated using measurement data obtained within the relative pressure (P/P0) range of 0.07–0.20. The C values for this calculation were found to be between 150 and 200.
[b] Pore volume is calculated by single point adsorption total pore volume of pores at P/P_0 0.99.
[c] Pore size is calculated by BJH method using desorption isotherm.

Table 2
Pt dispersion, adsorption volume of CO, Pt surface area and Pt particle size of catalyst. These properties were calculated by result of CO chemisorption experiments.

Sample	D (%) [a]	V_{ads} (cm^c/g) [b]	S_{Pt} (m^b/g) [c]	d_{Pt} (nm) [d]
0.01PtA	70.4	0.01	0.02	1.6
0.05PtA	41.2	0.02	0.05	2.7
0.5PtA	43.3	0.25	0.53	2.6
1PtA	37.2	0.43	0.92	3.0
3PtA	35.9	1.24	2.66	3.2

[a] Pt dispersion calculated based on CO adsorption amount and actual Pt amount in catalyst.
[b] CO adsorption amount measured by CO chemisorption.
[c] Pt metal surface area calculated based on the result of CO chemisorption.
[d] Pt particle size calculated based on the result of CO chemisorption.

Table 3
Pt amount measured by XRF and ICP-AES.

Sample	Pt_{XRF}(wt.%) [a]	$Pt_{ICP\text{-}AES}$(wt.%) [b]
0.01PtA	0.02	0.01
0.05PtA	0.06	0.05
0.5PtA	0.50	0.37
1PtA	0.95	0.86
3PtA	3.36	2.63

[a] Pt amount measured by XRF.
[b] Pt amount measured by ICP-AES.

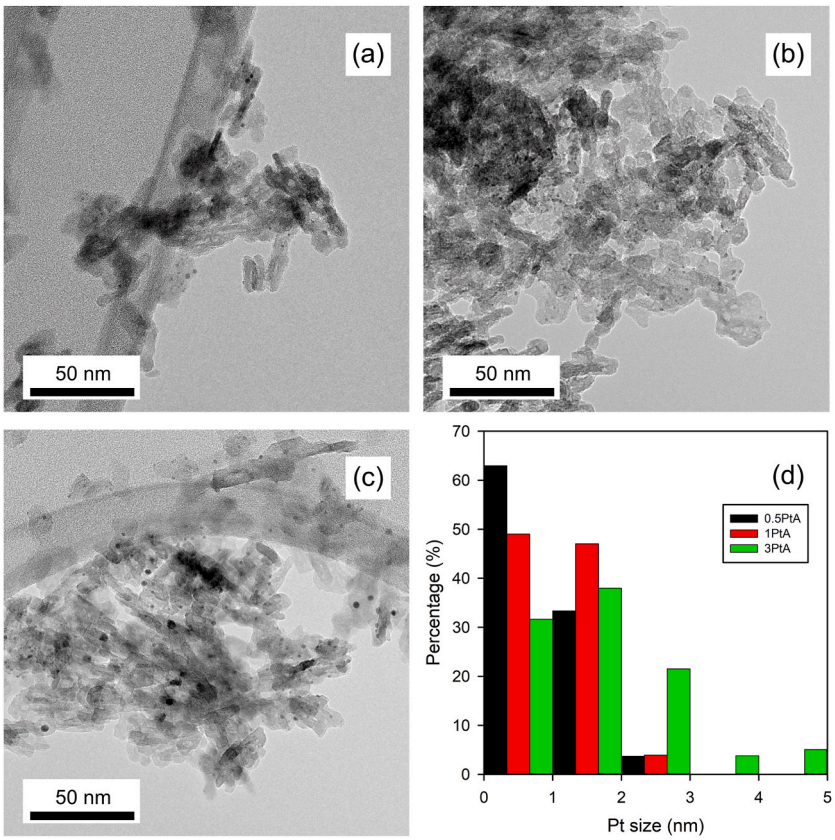

Fig. 2. TEM image of (a) 0.5PtA, (b) 1PtA, and (c) 3PtA catalyst and (d) particle size distribution of three samples that black, red and green bars present 0.5PtA, 1PtA and 3PtA, respectively.

3.2. Catalyst performance

3.2.1. Effect of Pt loading

The catalyst under study was assessed for its NOx reduction performance using toluene as a reducing agent under conditions conducive to high reduction. The evaluation of the catalysts, identified as 0.01PtA and 0.05PtA, revealed no detectable NOx conversion, as depicted in Fig. 3a. However, increasing the Pt loading to the 0.5PtA configuration resulted in a modest NOx conversion rate of 4.3 %. More significant improvements were observed with further increases in Pt content; 1PtA and 3PtA catalysts achieved NOx conversion rates of 16.2 % and 52.9 %, respectively, with 3PtA catalyst demonstrating the most effective de-NOx activity. These results suggest that higher Pt loadings enhance NOx reduction, although this also increases the cost of the catalyst. A comparison of catalytic performance based on the same Pt loading is provided in Table S1. While the NOx reduction rate of 1PtA was 1.5–2 times higher than that of 0.5PtA, the rates for 3PtA and 1PtA were nearly equivalent, indicating that the NOx reduction efficiency per unit of Pt becomes saturated at higher loadings.

While catalytic experiments, THC was also simultaneously monitored to evaluate toluene conversion efficiency which showed minimal activity (less than 3 %) for the 0.01PtA, 0.05PtA, and 0.5PtA catalysts in Fig. 3b. In contrast, the 1PtA catalyst achieved a toluene conversion rate of 6.6 %, and 3PtA catalyst exhibited a significantly higher conversion rate of 32.4 %. These findings indicate that increased Pt loadings enhance both NOx and toluene reduction efficiencies, suggesting a positive correlation between Pt content and catalytic performance. Similar trends have been reported in the literature, where the conversion rates of long-chain hydrocarbons and aromatic compounds, such as naphthalene, also increased with higher Pt loadings [66].

3.2.2. Effect of toluene concentration

Through a series of experiments using catalysts with varying Pt amounts, the catalyst designated as 3PtA demonstrated the most effective performance. This section focuses on evaluating the impact of operational conditions, including variations in toluene, NO, O_2 concentrations, and GHSV. In this series of experiments, toluene concentration was varied with other experimental conditions were constant, as shown in Fig. 4. Initially, in the absence of toluene, no NOx reduction was observed; instead, all NO was converted to NO_2

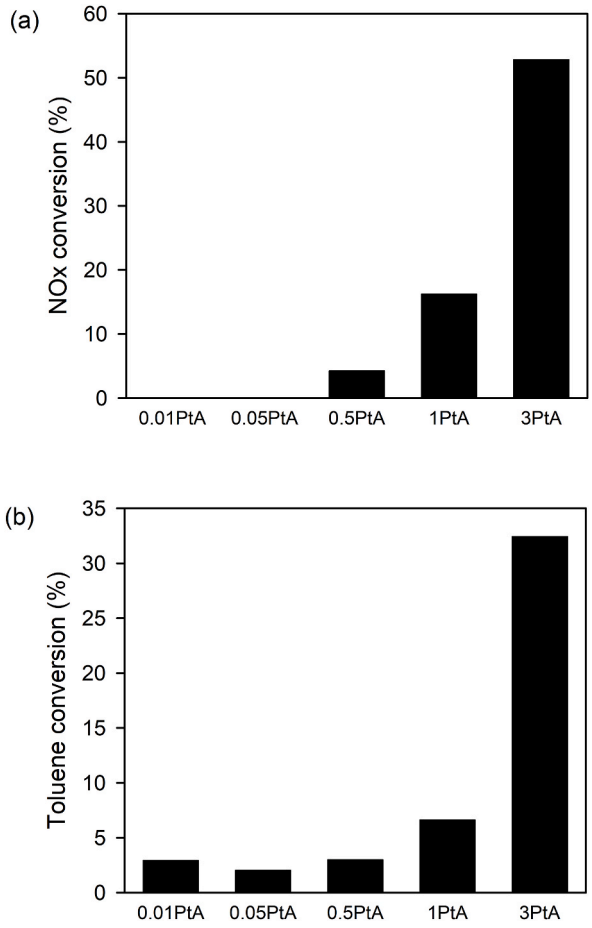

Fig. 3. (a) NOx and (b) toluene conversions of prepared catalysts which Pt loading is varied from 0.01 to 3 wt%. In the reactor, 20 mL catalysts were loaded and GHSV was 30,000 h^{-1}. Catalyst was tested at 250 °C in 1 % O_2, 5 % CO_2, 300 ppm NO and 30,000 ppm THC by injection of toluene.

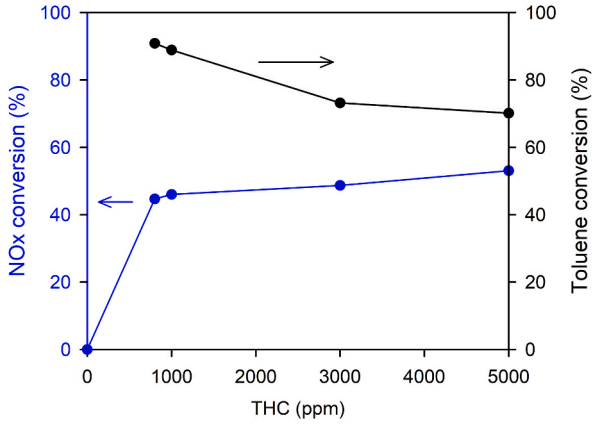

Fig. 4. NOx (blue) and toluene (black) conversions over 3PtA catalyst varying THC concentration from 800 to 5000 ppm including in the absence of toluene condition. In the reactor, 20 mL catalyst was loaded and GHSV was 30,000 h^{-1}. Catalyst was tested at 250 °C in 1 % O_2, 5 % CO_2, 150 ppm NO and 800 ppm THC by injection of toluene.

due to O_2 present in the feed. However, as THC concentration was increased from 800 to 5000 ppm, a notable increase in NOx conversion from 44.7 % to 53.1 % was recorded. This trend highlights the significant role of toluene as a reductant in the NOx reduction process.

In contrast, toluene conversion gradually decreased from 90.9 % at 800 ppm THC to 70.1 % at 5000 ppm THC. This decrease of conversion is attributed to the disproportionately large volume of toluene relative to the catalyst volume. Although toluene serves as an effective reducing agent, excessively high concentration does not proportionally enhance NOx reduction. This may be due to the difference of reactions' rate between NOx reduction by toluene and toluene oxidation, which likely imposes a limit on the effectiveness of the reaction between NOx and the hydrocarbon fragments derived from toluene.

3.2.3. Effect of NO concentration

NO concentration in the feed was varied between 50 and 500 ppm to simulate different operational conditions in facilities in Fig. 5. At 50 ppm, the catalyst achieved optimal de-NOx performance, with NOx conversion rate of 60.4 % and toluene conversion rate of 91.8 %. However, as NO feed concentration increased, there was a noticeable decrease in NOx conversion: 45.4 % at 100 ppm and 44.7 % at 150 ppm. When NO feed concentration exceeded 300 ppm, NOx conversion decreased significantly: down to 11 % at 300 ppm and 5.6 % at 500 ppm. Conversely, toluene conversion exhibited only a slight decrease; it was 89.8 % at 300 ppm and 89.4 % at 500 ppm. These results suggest that the reduction in NOx conversion with increasing NO feed concentration is due to competitive reactions between toluene oxidation and NOx reduction. Toluene oxidation appears to be more favored over NOx reduction by toluene, leading to a more pronounced decrease in NOx conversion relative to toluene conversion as NO feed concentration increases.

3.2.4. Effect of oxygen concentration

In experiments where toluene was absent, all NO was converted to NO_2 without any reduction to N_2, indicating that the presence of O_2 is a significant factor in NOx reduction by toluene in Fig. 6. To investigate this, we varied the O_2 concentration from 1 % to 5 %,

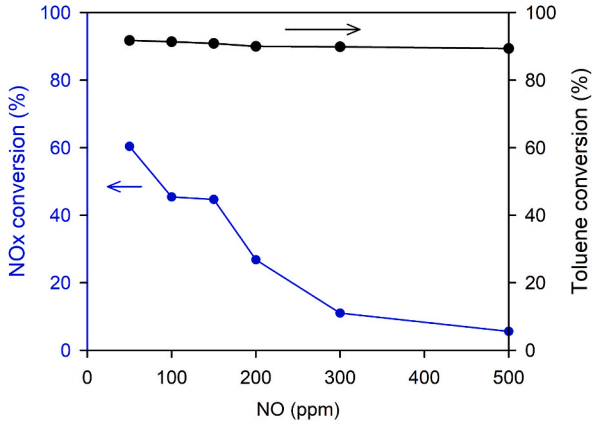

Fig. 5. NOx (blue) and toluene (black) conversions over 3PtA catalyst varying NO concentration from 50 to 500 ppm. In the reactor, 20 mL catalysts were loaded and GHSV was 30,000 h^{-1}. Catalyst was tested at 250 °C in 1 % O_2, 5 % CO_2 and 800 ppm THC by injection of toluene.

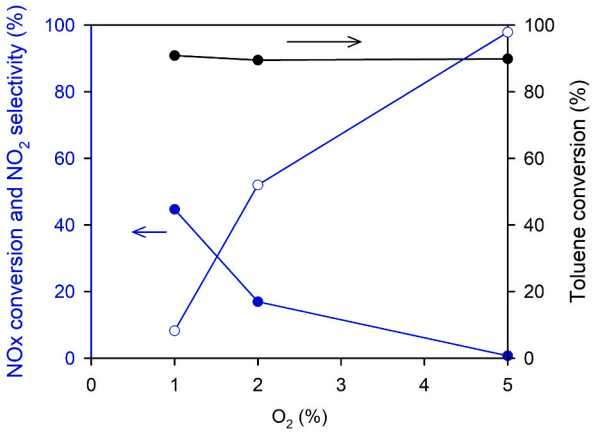

Fig. 6. NOx (blue filled circle) and toluene (black filled circle) conversions and NO_2 selectivity (blue open circle) over 3PtA catalyst varying O_2 concentration from 1 % to 5 %. In the reactor, 20 mL catalysts were loaded and GHSV was 30,000 h^{-1}. Catalyst was tested at 250 °C in 5 % CO_2, 150 ppm NO and 800 ppm THC by injection of toluene.

while keeping other reaction conditions constant. In the experiment with 1 % O_2, NOx reduction was observed at 44.7 %, but it drastically reduced to 16.9 % under 2 % O_2 conditions. Moreover, almost no NOx reduction was noted in the presence of 5 % O_2. Interestingly, toluene conversion remained relatively stable, ranging between 89 % and 90 %, suggesting that O_2 concentration does not significantly influence toluene oxidation. Focusing on NO_2 concentration, NO_2 selectivity was found to be 8.2 % at 1 % O_2 concentration. However, this selectivity increased markedly to 52 % and 97.9 % for 2 % and 5 % O_2 concentrations, respectively. This suggests that higher O_2 concentrations primarily affect the NOx reduction process, particularly promoting NO oxidation to NO_2 when toluene oxidation is not a factor. Similar trends have been reported in the literature, where O_2 concentrations are shown to proportionally influence NO oxidation to NO_2 [67–69].

3.2.5. *Effect of GHSV*

In a series of experiments conducted under varying reaction conditions, it was observed that feed concentrations have a significant impact on NOx reduction. Consequently, we considered that de-NOx performance should also be evaluated under different GHSV due to the complexity of the reaction dynamics in Fig. 7. When GHSV was increased from 5000 to 30,000 h^{-1}, a notable decrease in NOx conversion was observed, from 74 % to 44.7 %. In contrast, toluene conversion remained relatively stable, within the range of 80–90 %.

These findings suggest that the oxidation of toluene is a comparatively faster reaction than NOx reduction. Therefore, the variance in NOx conversion with changing GHSV is likely due to the differing reaction rates. The faster reaction rate of toluene oxidation means that it is less affected by the changes in GHSV compared to NOx reduction.

3.2.6. *Effect of reaction temperature*

The impact of reaction temperature on catalyst performance was also investigated under conditions of high THC content.

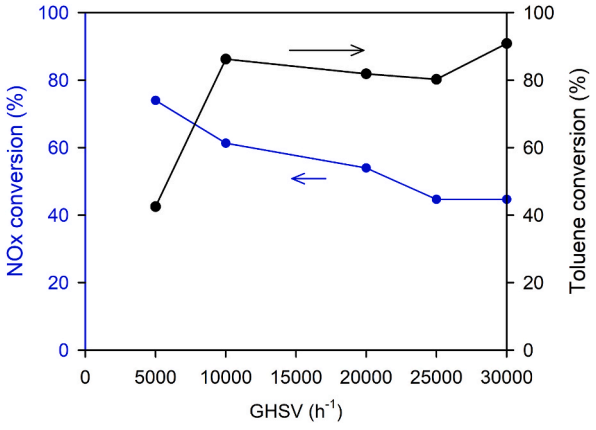

Fig. 7. NOx (blue) and toluene (black) conversions over 3PtA catalyst varying GHSV from 5000 to 30,000 h^{-1}. In the reactor, 20 mL catalysts were loaded and GHSV was controlled by total flow rate. Catalyst was tested at 250 °C in 5 % CO_2, 150 ppm NO and 800 ppm THC by injection of toluene.

Temperature control ranged from 200 to 400 °C in an environment with abundant THC in Fig. 8. At 200 °C, the catalyst achieved only 3.9 % NOx reduction and 2.9 % toluene conversion, suggesting that this temperature is too low for effective reactions with NOx and toluene. However, as the temperature was increased, the catalytic performance for NOx reduction improved significantly, reaching 78.7 % at 400 °C. Concurrently, toluene conversion 32.4 % was observed, influenced by the high toluene feed condition. These experiments were carried out under a constant NO concentration of 300 ppm and THC 30,000 ppm.

Comparison was also made with a lower THC 800 ppm, where toluene conversion significantly increased to 89.9 %. Additionally, experiments were conducted at a reduced NO 150 ppm, while maintaining the same THC level. Toluene conversion in this setup was 90.9 %, indicating that the difference in conversion was less than 1 % between the two THC conditions. However, NOx conversion was consistent at 44.7 % under both low NO and low THC conditions. These results suggest several conclusions: 1) Lower THC conditions are conducive to higher toluene conversion; 2) An optimal, rather than an excessive, THC concentration is necessary for effective NOx reduction; and 3) A reaction temperature above 300 °C is essential to facilitate NOx reduction using toluene as a reductant.

3.2.7. Short stress test in high-burden condition

Through extensive experiments, we identified the optimal conditions for maximizing NOx reduction performance. It was established that a higher Pt content in the catalyst is beneficial for reducing NOx. Consequently, 3PtA catalyst, with its higher Pt loading, was selected for further study. Meanwhile, the 1PtA catalyst was tested under a SO_2 containing gas mixture, as shown in Fig. S3. The catalytic performance decreased with increasing SO_2 concentration. Typically, the SO_2 concentration is less than 10 ppm when the fuel gas is LNG, but it can vary from tens to hundreds of ppm depending on the fuel source, such as byproduct gas or flue gas from processes. In this study, we could not test all process conditions; therefore, a gas mixture without SO_2 was used. The temperature was set at 450 °C, as temperatures above 300 °C had previously demonstrated effective de-NOx performance with the 3PtA catalyst. Although lower NO feed amounts generally favor NOx reduction, the concentration was set at 400 ppm to demonstrate the reaction's feasibility under more challenging conditions. Given the substantial NO concentration in the feed, THC concentration was adjusted to 10,000 ppm. Additionally, the oxygen concentration was controlled at 1 %, and GHSV was maintained at 30,000 h^{-1}.

This experimental setup represents a particularly strenuous condition due to the high concentrations of NO and toluene combined with a high GHSV. Despite these challenging circumstances, the 3PtA catalyst displayed impressive NOx conversion rates, achieving 89.7 % initially and maintaining 87.2 % after 70 min, indicating a stability rate of 97.6 %. N_2O selectivity was less than 1 % and NO_2 was not detected in Fig. S4. Furthermore, toluene conversion was consistently observed in the range of 93 %–96 % in Fig. 9. These results strongly suggest that the 3PtA catalyst is highly effective for simultaneous NOx and toluene reduction, even under demanding conditions. The ability of 3PtA to maintain high conversion rates and stability under such conditions underscores its potential applicability in industrial settings where NOx and VOC reduction are required simultaneously.

After reaction, used catalyst was characterized to compare fresh one in Table S1. Pt amount, BET surface area, pore volume and pore diameter of catalyst showed less difference compared to fresh one. However, Pt dispersion conducted by CO chemisorption was reduced from 35.9 % to 24.1 %. Pt particle could be segregated due to high demanding condition which is both high concentration of NOx and toluene and high temperature. Although this reaction condition and changes of catalytic properties, catalytic performance didn't show drastic deactivation.

The de-NOx process utilizing toluene encompasses three principal reactions: NOx reduction by toluene, toluene oxidation, and NO oxidation [70]. These reactions are integral to the domain of automobile exhaust treatment, where it is recognized that reductants with large molecular structures, such as aromatics and long-chain hydrocarbons, generally yield lower de-NOx efficiencies [71]. The limited effectiveness of these large molecules as reductants is linked to the necessity of breaking down their molecular structure over the catalyst, leading to the formation of smaller, reactive fragments that subsequently engage in reactions with NOx. This complex reaction

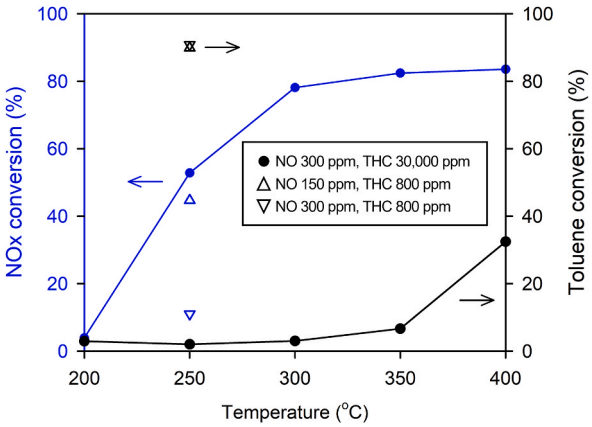

Fig. 8. NOx (blue filled circle) and toluene (black filled circle) conversions over 3PtA catalyst varying temperature from 200 to 400 °C. In the reactor, 20 mL catalysts were loaded and GHSV was 30,000 h^{-1}. Catalyst was tested at 250 °C in 5 % CO_2, 300 ppm NO and 30,000 ppm THC by injection of toluene. In addition, two different reaction conditions were conducted in NO 300 ppm and THC 800 ppm (downside triangle) and NO 150 ppm and THC 800 ppm (upside triangle).

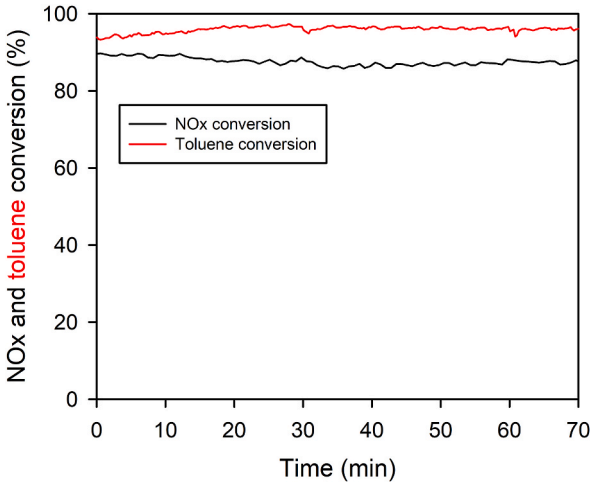

Fig. 9. NOx(blue line) and toluene (black line) conversions of 3PtA catalyst. In the reactor, 20 mL catalysts were loaded and GHSV was 30,000 h^{-1}. Catalyst was tested at 450 °C in 1 % O_2, 5 % CO_2, 150 ppm NO and 800 ppm THC by injection of toluene.

process leads to low de-NOx performance and less selective to reduced NOx. On the other hand, NH_3 and urea are known for highly selective reductant for de-NOx [72,73]. For this reason, in automotive applications, these reductants are commonly employed as reductants.

In contrast to automotive systems, small size facilities often have greater flexibility in terms of capacity and operational temperature range. This flexibility has able to present a significant advantage in using VOCs present in flue gas as reductants, without the need for additional NH_3 injection, despite the initial activation time required. Such an approach can be particularly advantageous in settings where the integration of additional reductant injection systems is impractical or financially burdensome. By leveraging the intrinsic components of the flue gas, these smaller facilities can effectively engage in the de-NOx process while optimizing resource utilization and minimizing operational complexities.

3.2.8. Preliminary process simulations compared to conventional methods

NOx reduction process utilizing toluene as a reducing agent was designed specifically for small-scale operations emitting both NOx and VOCs, as an alternative to the conventional approach, which typically combines RCO with NH_3 SCR. Preliminary simulations for both processes were conducted using Aspen HYSYS software (V11®, Aspen Technology, Inc., USA). The simulations utilized the component database available within HYSYS, and the Peng-Robinson equation of state was selected as the thermodynamic model. The following reactions were modeled: the oxidation of toluene ($C_7H_8 + 9O_2 \rightarrow 7CO_2 + 4H_2O$), the reduction of NO by toluene ($C_7H_8 + 18NO \rightarrow 7CO_2 + 4H_2O + 9N_2$), and the reduction of NO by ammonia ($4NO + 4NH_3 + O_2 \rightarrow 4N_2 + 6H_2O$). The detail simulation results are shown in Table S2.

As shown in Fig. 10a, the NOx reduction process using toluene consists of a single catalytic reactor, two heat exchangers, and one heater. NOx and THC conversions were set at 90 % and 97 %, respectively, based on short-duration stress tests. The reactor inlet temperature was set at 450 °C, with an outlet temperature of 463 °C, due to the exothermic nature of both NOx reduction by toluene and toluene oxidation reactions. To optimize energy efficiency, two heat exchangers were employed to preheat the feed stream, and a heater was used to achieve the required reaction temperature. The heat duty for the heater was calculated to be 203.8 MJ/h.

In contrast, Fig. 10b depicts the conventional process, which assumes the use of RCO in combination with NH_3 SCR for the reduction of toluene and NOx. In this configuration, the feed gas first enters the adsorption section of RCO to reduce toluene. The gas then passes through two heat exchangers and a heater, with NH_3 injection, to reach the required reaction temperature for NOx reduction over a conventional SCR catalyst, where the NOx removal efficiency was assumed to be 95 %. In the desorption section of RCO, air is preheated via a heat exchanger connected to the oxidation reactor. The exothermic nature of the toluene oxidation reaction raises the temperature of the air. The desorbed toluene, after further heating, reaches the reaction temperature and is converted to CO_2 and H_2O in the reactor, with an assumed conversion efficiency of 95 %. Toluene adsorption efficiency was also assumed to be 95 %, with other components assumed at 1 %. This conventional process model comprises two reactors, two heaters, and three heat exchangers. The heat duties for heater-1 and heater-2 were calculated to be 220.0 MJ/h and 2.3 MJ/h, respectively, resulting in a total heat duty of 222.3 MJ/h.

The developed process in this study requires 8.3 % less heat duty compared to the conventional process. Additionally, the proposed process has a simpler configuration, utilizing only four pieces of equipment compared to the seven in the conventional method. Moreover, this process eliminates the need for an additional reducing agent, simplifying the configuration further. The use of NH_3 in conventional systems necessitates additional equipment such as injection pumps, storage tanks, and emergency scrubbers. Furthermore, NH_3 is typically classified as a regulated chemical, requiring specialized equipment to comply with government regulations, including high-pressure systems and licensing requirements.

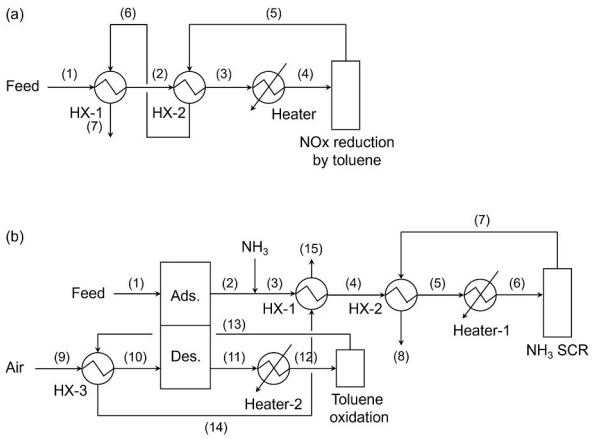

Fig. 10. Process scheme of NOx reduction by toluene and conventional process consisting of RCO and NH_3 SCR. The stream is marked as number and its information such as temperature, flow rate and composition is shown in Table S2.

4. Conclusions

In this study, both NOx and VOCs were reduced over single Pt-based catalyst. Toluene, a common solvent in industrial processes, was used as a model VOCs. Through preparation of several catalysts and performance tests, it reveals that higher Pt loadings improved NOx reduction efficiency. Notably, 3PtA catalyst exhibited outstanding performance, maintaining high NOx and toluene conversion rates even under high-burden conditions. The experiments conducted under different operational conditions, such as varying NO, toluene, O_2, GHSV and temperature, demonstrated that feed conditions significantly impact NOx reduction. The results indicated that toluene oxidation occurs at a faster rate than NOx reduction, affecting the overall efficiency of the process. In conclusion, the study successfully identified optimal conditions for NOx and VOC reduction using Pt-based catalysts. In particular, 3PtA catalyst, showed high efficacy in simultaneously reducing NOx (89.7 % NOx conversion) and toluene (93.3 %), even in challenging scenarios with high NO and toluene concentrations and GHSV. Additionally, the NOx reduction process using toluene was found to be 8 % more energy-efficient compared to the conventional combined RCO and NH_3 SCR processes. These findings pave the way for applying such catalysts in industrial settings, offering a viable solution for reducing the environmental footprint of industrial activities and improving public health outcomes.

CRediT authorship contribution statement

Cheonwoo Jeong: Writing – original draft, Visualization, Validation, Supervision, Methodology, Investigation, Funding acquisition, Conceptualization. **Dongcheol Lee:** Writing – review & editing, Validation, Investigation. **Sungjoong Kim:** Methodology, Investigation. **Joon Hyun Baik:** Writing – review & editing, Validation. **Joonwoo Kim:** Writing – review & editing, Validation, Supervision, Project administration, Funding acquisition, Conceptualization.

Declaration of competing interest

The authors declare the following financial interests/personal relationships which may be considered as potential competing interests: Cheonwoo Jeong reports financial support was provided by Korea Evaluation Institute of Industrial Technology. Joonwoo Kim reports financial support was provided by Korea Evaluation Institute of Industrial Technology. Cheonwoo Jeong has patent #10-2023-0181459 issued to Research Institute of Industrial Science & Technology. If there are other authors, they declare that they have no known competing financial interests or personal relationships that could have appeared to influence the work reported in this paper.

Acknowledgements

This work was supported by the Korea Evaluation Institute of Industrial Technology through the Ministry of Trade, Industry and Energy (Alchemist Project 20018904, NTIS-141518011 and project No. 20015736).

Appendix A. Supplementary data

Supplementary data to this article can be found online at https://doi.org/10.1016/j.heliyon.2024.e40625.

References

[1] K. Skalska, J.S. Miller, S. Ledakowicz, Trends in NOx abatement: a review, Sci. Total Environ. 408 (2010) 3976–3989.
[2] R.K. Srivastava, W. Neuffer, D. Grano, S. Khan, J.E. Staudt, W. Jozewicz, Controlling NOx emission from industrial sources, Environ. Prog. 24 (2005) 181–197.
[3] U. Asghar, S. Rafiq, A. Anwar, T. Iqbal, A. Ahmed, F. Jamil, M.S. Khurram, M.M. Akbar, A. Farooq, N.S. Shah, Y.-K. Park, Review on the progress in emission control technologies for the abatement of CO_2, SOx and NOx from fuel combustion, J. Environ. Chem. Eng. 9 (2021) 106064.
[4] D.N. Cao, A.T. Hoang, H.Q. Luu, V.G. Bui, T.T.H. Tran, Effects of injection pressure on the NOx and PM emission control of diesel engine: a review under the aspect of PCCI combustion condition, Energy Sources: Recovery Util. Environ. Eff. 46 (2020) 7414–7431.
[5] J.-C. Kim, Trends and control technologies of volatile organic compound, J. Korean Soc. Atmos 22 (2006) 743–757.
[6] Z. Xu, Y. Li, H. Shi, Y. Lin, Y. Wang, Q. Wang, T. Zhu, Application prospect of K used for catalytic removal of NOx, COx, and VOCs from industrial flue gas: a review, Catalysts 11 (2021) 419.
[7] X. Zhou, J. Xie, R. Zhang, M. Ma, X. Li, P. Gong, Recent advances in different catalysts for synergistic removal of NOx and VOCs: a minor review, J. Environ. Chem. Eng. 12 (2024) 111764.
[8] Z. Zhao, S. Ma, B. Gao, F. Bi, R. Qiao, Y. Yang, M. Wu, X. Zhang, A systematic review of intermediates and their characterization methods in VOCs degradation by different catalytic technologies, Sep. Purif. Technol. 314 (2023) 123510.
[9] A. Fayyazbakhsh, M.L. Bell, X. Zhu, X. Mei, M. Koutný, N. Hajinajaf, Y. Zhang, Engine emissions with air pollutants and greenhouse gases and their control technologies, J. Clean. Prod. 376 (2022) 134260.
[10] D.G. Streets, S.T. Waldhoff, Present and future emissions of air pollutants in China: SO_2, NOx, and CO, Atmos. Environ. 34 (2000) 363–374.
[11] H.C. Frey, J. Zheng, Quantification of variability and uncertainty in air pollutant emission inventories: method and case study for utility NOx emissions, J. Air Waste Manag. Assoc. 52 (2002) 1083–1095.
[12] A.C.G. César, J.A. Carvalho Jr, L.F.C. Nascimento, Association between NOx exposure and deaths caused by respiratory diseases in a medium-sized Brazilian city, Braz. J. Med. Biol. Res. 48 (2015) 1130–1135.
[13] W. Vries, Impacts of nitrogen emissions on ecosystems and human health: a mini review, Curr. Opin. Environ. Sci. Health 21 (2021) 100249.
[14] J.G. Irwin, M.L. Williams, Acid rain: chemistry and transport, Environ. Pollut. 50 (1988) 29–59.
[15] D. Vadel, A Study of Spatial Distribution of Ozone and its Correlation with Meteorological Parameters and Precursors, Oklahoma State University, 2005.
[16] H. Simon, A. Reff, B. Wells, J. Xing, N. Fran, Ozone trends across the United States over a period of decreasing NOx and VOC emissions, Environ. Sci. Technol. 49 (2015) 186–195.
[17] S.H.A. Rizvi, P. Agrawal, S. Batra, N. Nidhi, V. Singh, Assessing urban heat island intensity and emissions with compressed natural gas in non-commercial vehicles, Urban Clim. 48 (2023) 101421.
[18] M.S. Kamal, S.A. Razzak, M.M. Hossain, Catalytic oxidation of volatile organic compounds (VOCs)-A review, Atmos. Environ. 140 (2016) 117–134.
[19] C. He, J. Cheng, X. Zhang, M. Douthwaite, S. Pattisson, Z. Hao, Recent advances in the catalytic oxidation of volatile organic compounds, Chem. Rev. 119 (7) (2019) 4471–4568.
[20] W.P. Carter, Development of ozone reactivity scales for volatile organic compounds, J. Air Waste Manage. Assoc. 44 (1994) 881–899.
[21] R. Atkinson, Atmospheric chemistry of VOCs and NOx, Atmos. Environ. 34 (2000) 2063–2101.
[22] H. Zhao, P. Meng, S. Gao, Y. Wang, P. Sun, Z. Wu, Recent advances in simultaneous removal of NOx and VOCs over bifunctional catalysts via SCR and oxidation reaction, Sci. Total Environ. 906 (2023) 167553.
[23] B. McDonald, J.A. De Gouw, J.B. Gilman, S.H. Jather, A. Akherati, C.D. Cappa, M. Trainer, Volatile chemical products emerging as largest petrochemical source of urban organic emissions, Science 357 (6377) (2018) 760–764.
[24] J.H. Kim, J.H. Kim, H.S. Kim, H.J. Kim, S.H. Kang, J.H. Ryu, S.S. Shim, Reduction of NOx emission from the cement industry in South Korea: a review, Atmosphere 13 (1) (2022) 121.
[25] D.I. Lee, Trends of Future Technologies for Heavy-Duty Diesel Engine, Engine R&D Center, Daewoo Heavy Industries & Machinery Ltd, 2003, pp. 58–65.
[26] Y. Fu, Q. Xin, S. Zhang, Y. Yang, Simultaneous catalytic removal of VOCs and NOx, Aerosol Air Qual. Res. 21 (12) (2021) 210214.
[27] L. Han, S. Cai, M. Gao, J.Y. Hasegawa, P. Wang, J. Zhang, D. Zhang, Selective catalytic reduction of NOx with NH3 by using novel catalysts: state of the art and future prospects, Chem. Rev. 119 (19) (2019) 10916–10976.
[28] G. Busca, L. Lietti, G. Ramis, F. Berti, Chemical and mechanistic aspects of the selective catalytic reduction of NOx by ammonia over oxide catalysts: a review, Appl. Catal. B Environ. 18 (1998) 1–36.
[29] B. Guan, R. Zhan, H. Lin, Z. Huang, Review of state-of-the-art technologies of selective catalytic reduction of NOx from diesel engine exhaust, Appl. Therm. Eng. 66 (2014) 395–414.
[30] B.V. Ramabrahmam, B. Sreenivasulu, M.M. Mallikarjunan, Model on-site emergency plan. Case study: toxic gas release from an ammonia storage terminal, J. Loss Prev. Process. Ind. 9 (4) (1996) 259–265.
[31] Z. Zhang, Z. Jiang, W. Shangguan, Low-temperature catalysis for VOCs removal in technology and application: a state-of-the-art review, Catal. Today 264 (2016) 270–278.
[32] B.R. Kim, VOC emissions from automotive painting and their control: a review, Environ. Eng. Res. 16 (2011) 1–9.
[33] B.S. Choi, J. Yi, Simulation and optimization on the regenerative thermal oxidation of volatile organic compounds, Chem. Eng. J. 76 (2000) 103–114.
[34] M. Tomatis, M.T. Moreira, H. Xu, W. Deng, J. He, A.M. Parvez, Removal of VOCs from waste gases using various thermal oxidizers: a comparative study based on life cycle assessment and cost analysis in China, J. Clean. Prod. 233 (2019) 808–818.
[35] D.A. Lewandowski, Design of Thermal Oxidation Systems for Volatile Organic Compounds, CRC press, 2017.
[36] B. Sauer, W. Franklin, R. Miner, D. Word, B. Upton, Environmental tradeoffs: life cycle approach to evaluate the burdens and benefits of emission control systems in the wood panel industry, For. Prod. J. 52 (2002) 50.
[37] R. Neitzel, N. Seixas, K. Ren, A review of crane safety in the construction industry, Appl. Occup. Environ. Hyg 16 (2010) 1106–1117.
[38] M.A. Habib, M. Elshafei, M. Dajani, Influence of combustion parameters on NOx production in an industrial boiler, Comput. Fluids 37 (2008) 12–23.
[39] J. Morin, A. Gandolfo, B. Temime-Roussel, R. Strekowski, G. Brochard, V. Berge, H. Wortham, Application of a mineral binder to reduce VOC emissions from indoor photocatalytic paints, Build. Environ. 156 (2019) 225–232.
[40] S.H. Kim, D.J. Seo, H.R. Kim, J.H. Park, K.W. Lee, S.J. Bae, H.M. Song, Estimation and analysis of VOCs emissions from painting and printing facilities in industrial complexes of Gwangju, J. Environ. Sci. Int. 29 (5) (2020) 479–494.
[41] G.R. Parmar, N.N. Rao, Emerging control technologies for volatile organic compounds, Crit. Rev. Environ. Sci. Technol. 39 (2009) 41–78.
[42] T. Wei, C. Ma, Y. Wen, H. Yue, S. Yang, J. Zhao, X. Wang, An integrated biological system for air pollution control in WtE plants and interaction between NO reduction and toluene oxidation, J. Clean. Prod. 335 (2022) 131792.
[43] J. Zhu, Y. Cheng, Z. Wang, J. Zhang, Y. Yue, G. Qian, Low-energy production of a monolithic catalyst with MnCu-synergetic enhancement for catalytic oxidation of volatile organic compounds, J. Environ. Manage. 336 (2023) 117688.
[44] B.S. Seo, E.H. Ko, B. Kim, N.K. Park, S.B. Kang, D. Kang, M. Kim, Computational screening-based development in VOC removal catalyst: methyl ethyl ketone oxidation over Pt/TiO_2, Chem. Eng. J. 452 (2023) 139466.
[45] A. Ayyagari, V. Hasannaeimi, H.S. Grewal, H. Arora, S. Mukherjee, Corrosion, erosion and wear behavior of complex concentrated alloys: a review, Metals 8 (2018) 603.
[46] M. Iwamoto, H. Yahiro, Novel catalytic decomposition and reduction of NO, Catal. Today 22 (1994) 5–18.
[47] A. Frobert, S. Raux, A. Lahougue, C. Hamon, K. Pajot, G. Blanchard, HC-SCR on silver-based catalyst: from synthetic gas bench to real gas, SAE Int. J. Fuels Lubr. 5 (2012) 389–398.
[48] J. Kim, J. Lee, E. Kim, H. Han, Optimization of HC-SCR catalysts for enhancing the DeNOx efficiency, KSAE Spring Conference Proceedings 5 (2011) 454–456.

[49] G. Xiao, Z. Guo, B. Lin, M. Fu, D. Ye, Y. Hu, Cu-VWT catalysts for synergistic elimination of NOx and volatile organic compounds from coal-fires flue gas, Environ. Sci. Technol. 56 (2022) 10095–10104.
[50] G. Xiao, Z. Guo, J. Li, Y. Du, Y. Zhang, T. Xiong, B. Lin, M. Fu, D. Ye, Y. Hu, Insights into the effect of flue gas on synergistic elimination of toluene and NOx over V_2O_5-$MoO_3(WO_3)/TiO_2$ catalysts, Chem. Eng. J. 435 (2022) 134914.
[51] G. Li, L. Wang, P. Wu, S. Zhang, K. Shen, Y. Zhang, Insight into the combined catalytic removal properties of Pd modification V/TiO_2 catalysts for the nitrogen oxides and benzene by: an experiment and DFT study, Appl. Surf. Sci. 527 (2020) 146787.
[52] N. Aoun, A. Schlange, A.R. Santos, U. Kunz, T. Turek, Effect of the OH−/Pt ratio during polyol synthesis on metal loading and particle size in DMFC catalysts, Electrocatalysis 7 (1) (2015) 13–21.
[53] T. Lagarteira, S. Delgado, C. Fernandes, C. Azenha, C. Mateos-Pedrero, A. Mendes, The role of Pt loading on reduced graphene oxide support in the polyol synthesis of catalysts for oxygen reduction reaction, Int. J. Hydrog. Energy 45 (40) (2020) 20594–20604.
[54] D.C. Lee, H.N. Yang, S.H. Park, W.J. Kim, Nafion/graphene oxide composite membranes for low humidifying polymer electrolyte membrane fuel cell, J. Membr. Sci. 452 (2014) 20–28.
[55] Y.Y. Chu, Z.B. Wang, D.M. Gu, G.P. Yin, Performance of Pt/C catalysts prepared by microwave-assisted polyol process for methanol electrooxidation, J. Power Sources 195 (2010) 1799–1804.
[56] N. Li, S. Tang, Y. Pan, X. Meng, One-step and rapid synthesis of reduced graphene oxide supported Pt nanodendrites by a microwave-assisted simultaneous reduction, Mater. Res. Bull. 49 (2014) 119–125.
[57] X. Liu, J. Duan, H. Chen, Y. Zhang, X. Zhang, A carbon riveted Pt/Graphene catalyst with high stability for direct methanol fuel cell, Microelectron. Eng. 110 (2013) 354–357.
[58] M. Sun, A.E. Nelson, J. Adjaye, Examination of spinel and non-spinel structural models for γ-Al_2O_3 by DFT and Rietveld refinement simulations, J. Phys. Chem. B 110 (2006) 20724–20726.
[59] Y. Rozita, R. Brydson, A.J. Scott, An investigation of commercial gamma-Al_2O_3 nanoparticles, J. Phys. Conf. Ser. 241 (2010) 012096.
[60] R. Prins, On the structure of γ-Al_2O_3, J. Catal. 392 (2020) 336–346.
[61] J. Lee, E.J. Jang, D.G. Oh, J. Szanyi, J.H. Kwak, Morphology and size of Pt on Al2O3: the role of specific metal-support interactions between Pt and Al_2O_3, J. Catal. 385 (2020) 204–212.
[62] C. Meephoka, C. Chaisuk, P. Samparnpiboon, P. Praserthdam, Effect of phase composition between nano γ- and χ-Al_2O_3 on Pt/Al_2O_3 catalyst in CO oxidation, Catal. Commun. 9 (2008) 546–550.
[63] H. Liu, G. Lu, Y. Guo, Y. Wang, Y. Guo, Synthesis of mesoporous Pt/Al_2O_3 catalysts with high catalytic performance for hydrogenation of acetophenone, Catal. Commun. 10 (2009) 1324–1329.
[64] G. Ertl, M. Neumann, K.M. Streit, Chemisorption of CO on the Pt (111) surface, Surf. Sci. 64 (1977) 393–410.
[65] H.C. Yao, M. Sieg, H.K. Plummer, Surface interactions in the Pt/γ-Al_2O_3 system, J. Catal. 59 (1979) 365–374.
[66] F. Diehl, J. Barbier, D. Duprez, I. Guibard, G. Mabilon, Catalytic oxidation of heavy hydrocarbons over Pt/Al_2O_3. Oxidation of C_{10+} solid hydrocarbons representative of soluble organic fraction of Diesel soots, Appl. Catal. A 504 (2015) 37–48.
[67] B.M. Weiss, E. Iglesia, NO oxidation catalysis on Pt clusters: elementary steps, structural requirements, and synergistic effects of NO_2 adsorption sites, J. Phys. Chem. C 113 (2009) 13331–13340.
[68] S.S. Mulla, N. Chen, W.N. Delgass, W.S. Epling, F.H. Ribeiro, NO_2 inhibits the catalytic reaction of NO and O_2 over Pt, Catal. Lett. 100 (2005) 267–270.
[69] A.R. Salman, B.C. Enger, X. Auvray, R. Lødeng, M. Menon, D. Waller, M. Rønning, Catalytic oxidation of NO to NO_2 for nitric acid production over a Pt/Al_2O_3 catalyst, Appl. Catal. A 564 (2018) 142–146.
[70] H.S. Kim, S. Kasipandi, J. Kim, S.H. Kang, J.H. Kim, J.H. Ryu, J.W. Bae, Current catalyst technology of selective catalytic reduction (SCR) for NOx removal in South Korea, Catalysts 10 (2020) 52.
[71] C.E. Stere, W. Adress, R. Burch, S. Chansai, A. Goguet, W.G. Graham, C. Hardacre, Ambient temperature hydrocarbon selective catalytic reduction of NOx using Ag/Al_2O_3 catalyst, ACS Catal. 4 (2014) 666–673.
[72] F. Gramigni, U. Lacobone, N.D. Nasello, T. Selleri, N. Usberti, I. Nova, Review of hydrocarbon poisoning and deactivation effects on Cu-zeolite, Fe zeolite, and vanadium-based selective catalytic reduction catalysts for NOx removal from lean exhausts, Ind. Eng. Chem. Res. 60 (2021) 6403–6420.
[73] Z. Lin, F. Yu, C. Ma, J. Dan, J. Luo, B. Dai, A critical review of recent progress and perspective in practical denitration application, Catalysts 9 (2019) 771.